DTIC FILE COPY

AD-A225 866

A Sunspot Maximum Prediction
Using a Neural Network

H. C. KOONS and D. J. GORNEY
Space Sciences Laboratory
Laboratory Operations
The Aerospace Corporation
El Segundo, CA 90245

1 February 1990

Prepared for

SPACE SYSTEMS DIVISION
AIR FORCE SYSTEMS COMMAND
Los Angeles Air Force Base
P.O. Box 92960
Los Angeles, CA 90009-2960

DTIC
ELECTE
AUG 27 1990
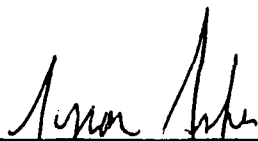D

This report was submitted by The Aerospace Corporation, El Segundo, CA 90245, under Contract No. F04701-88-C-0089 with the Space Systems Division, P.O. Box 92960, Los Angeles, CA 90009-2960. It was reviewed and approved for The Aerospace Corporation by H. R. Rugge, Acting Director, Space Sciences Laboratory.

Lt Fisher was the project officer for the Mission-Oriented Investigation and Experimentation (MOIE) Program.

This report has been reviewed by the Public Affairs Office (PAS) and is releasable to the National Technical Information Service (NTIS). At NTIS, it will be available to the general public, including foreign nationals.

This technical report has been reviewed and is approved for publication. Publication of this report does not constitute Air Force approval of the report's findings or conclusions. It is published only for the exchange and stimulation of ideas.

TYRON FISHER, LT, USAF
MOIE Project Officer
SSD/CLPO

RAYMOND M. LEONG, MAJ, USAF
MOIE Program Manager
AFSTC/WCO OL-AB

REPORT DOCUMENTATION PAGE

1a. REPORT SECURITY CLASSIFICATION Unclassified		1b. RESTRICTIVE MARKINGS			
2a. SECURITY CLASSIFICATION AUTHORITY		3. DISTRIBUTION/AVAILABILITY OF REPORT Approved for public release; distribution unlimited			
2b. DECLASSIFICATION/DOWNGRADING SCHEDULE					
4. PERFORMING ORGANIZATION REPORT NUMBER(S) TR-0090(5940-06)-1		5. MONITORING ORGANIZATION REPORT NUMBER(S) SSD-TR-90-16			
6a. NAME OF PERFORMING ORGANIZATION The Aerospace Corporation Laboratory Operations	6b. OFFICE SYMBOL (If applicable)	7a. NAME OF MONITORING ORGANIZATION Space Systems Division			
6c. ADDRESS (City, State, and ZIP Code) El Segundo, CA 90245-4691		7b. ADDRESS (City, State, and ZIP Code) Los Angeles Air Force Base Los Angeles, CA 90009-2960			
8a. NAME OF FUNDING/SPONSORING ORGANIZATION	8b. OFFICE SYMBOL (If applicable)	9. PROCUREMENT INSTRUMENT IDENTIFICATION NUMBER F04701-88-C-0089			
8c. ADDRESS (City, State, and ZIP Code)		10. SOURCE OF FUNDING NUMBERS			
		PROGRAM ELEMENT NO.	PROJECT NO.	TASK NO.	WORK UNIT ACCESSION NO.

11. TITLE (Include Security Classification)

A Sunspot Maximum Prediction Using a Neural Network

12. PERSONAL AUTHOR(S)
Koons, Harry C., and Gorney, David J.

13a. TYPE OF REPORT	13b. TIME COVERED FROM _____ TO _____	14. DATE OF REPORT (Year, Month, Day) 1 February 1990	15. PAGE COUNT 13

16. SUPPLEMENTARY NOTATION

17. COSATI CODES			18. SUBJECT TERMS (Continue on reverse if necessary and identify by block number)
FIELD	GROUP	SUB-GROUP	Neural Network Solar Cycle Sunspots

19. ABSTRACT (Continue on reverse if necessary and identify by block number)

Based on the rapid increase in the sunspot numbers for the current solar cycle, the current cycle (number 22) is expected to produce the largest number of major solar flares of any cycle in recent history. Since a number of different types of spacecraft anomalies are related to maxima in the solar activity, it is important to predict both the amplitude of the solar cycle and the time at which the maximum is expected to occur. We have taken a novel approach to making such a prediction. We have used Neural Network Simulation Software from California Scientific Software to predict the maximum 13-month-smoothed sunspot number for cycle 22 and the month in which this maximum will occur. The neural network predicts the maximum sunspot number for cycle 22 to be 194 ± 26, to occur 42 months (March 1990) after the minimum. The uncertainty in the prediction is taken to be the standard deviation of the difference between the predicted sunspot maximum and the observed sunspot maximum for 15 test cases taken from previous cycles. The prediction is in line with the predictions by NASA, 195 ± 40, to occur in February 1990, and by NOAA, Space Environment Laboratory, 203 ± 30, to occur in March 1990.

20. DISTRIBUTION/AVAILABILITY OF ABSTRACT ☐ UNCLASSIFIED/UNLIMITED ☒ SAME AS RPT. ☐ DTIC USERS	21. ABSTRACT SECURITY CLASSIFICATION Unclassified	
22a. NAME OF RESPONSIBLE INDIVIDUAL	22b. TELEPHONE (Include Area Code)	22c. OFFICE SYMBOL

DD FORM 1473, 84 MAR   83 APR edition may be used until exhausted.   SECURITY CLASSIFICATION OF THIS PAGE
All other editions are obsolete
UNCLASSIFIED

PREFACE

Data used in this study were provided by WDC-A for Solar-Terrestrial Physics, NOAA, Boulder, CO.

A-1

1

FIGURES

Solar activity near the maximum of each 11-year solar cycle causes a number of adverse effects on space systems. Satellites experience increased electrical charging of their surface and internal dielectric components, resulting in disruptive electrostatic discharges, and micro-electronic devices experience upsets more often. Satellite communications links in the very high frequency (VHF)/ultra high frequency (UHF) range suffer signal fades more often and with greater severity. The increased atmospheric density increases the drag on satellites at low altitudes, causing difficulties in tracking and in predicting their orbit decay and time of reentry. Because these effects are related to solar activity, it is important to predict both the amplitude of the solar cycle, measured by the maximum smoothed sunspot number, and the month in which the maximum is expected to occur. Solar cycles vary considerably in both the maximum sunspot number reached and the time after sunspot minimum that the maximum occurs.

Withbroe [1989] has recently reviewed solar cycle predictions for cycle 22. He notes that existing techniques can be divided into three broad categories--statistical, precursor, and McNish-Lincoln. Statistical techniques analyze the historical record for periodicities and trends. Precursor techniques correlate some parameters from the previous cycle or previous solar minimum with the sunspot number at the following maximum. Precursor techniques may use ad hoc relationships or may be founded on physical principles. An example of the latter is the prediction technique of Schatten et al. [1978] and Schatten and Sofia [1987], which shows that the sun's polar field strength near solar minimum is related to the following cycle's solar activity. The McNish-Lincoln technique is a "self-correcting" technique that relates the sunspot number N months after sunspot minimum to the mean for that month from preceding cycles and a correction term related to the departure of the current cycle from this mean [McNish and Lincoln, 1949].

We have taken a novel approach to making a sunspot prediction using a precursor technique. We have used BrainMaker, neural network simulation software from California Scientific Software, to predict the maximum 13-month-smoothed sunspot number for cycle 22 and the month in which this maximum will occur. The network software was run on a COMPAQ Deskpro 386 computer with a clock speed of 16 MHz. Neural networks can be trained to recognize complex patterns by association. In this application, the neural network is trained to recognize a pattern in the onset of a new sunspot cycle that can be used to predict the maximum sunspot number that will be reached and the number of months from the minimum to the maximum. Training times ranged from 15 to 30 min for each case.

The neural network used for this application consists of three layers of neurons, as shown in Fig. 1. There are 33 neurons (numbered 0 to 32) in the first layer connected to the input. The input consists of 33 months of 3-month-smoothed sunspot numbers. Month 1 is taken to be

5

Fig. 1.   The Architecture of the Neural Network Used to Predict the Maximum Sunspot Number for Solar Cycle 22

the month of the minimum of the 13-month-smoothed sunspot numbers preceding a cycle. There are 17 hidden neurons in the second layer, and there are two neurons in the third layer connected to the output. The first output is the maximum 13-month-smoothed sunspot number for the cycle, and the second output is the number of months from sunspot minimum to sunspot maximum for the cycle.

There are only connections between a neuron and neurons in the previous layer. Neurons in a given layer do not connect to each other and do not take inputs from subsequent layers or from layers before the previous one. So layer 1 sends outputs to layer 2, and layer 2 takes inputs from layer 1 and sends outputs to layer 3.

The connection strengths between any two layers constitute the elements of a real-valued matrix W. W_{ij} is the weight from neuron i (in some layer) to neuron j (in the next higher layer). The weights are the values that are modified by training.

The neural network uses a back propagation algorithm. Back propagation is a supervised learning scheme by which a layered feedforward network is trained to become a pattern matching engine. Training is accomplished by using a set of input/output pairs. The inputs consist of 33 known values and the outputs of 2 known values. In our application, data from previous sunspot cycles were used for training. Training uses a minimization algorithm, in this case, the method of steepest descent, to minimize the error between the output from the network and the known output values. Training consists of running patterns through the network in the forward direction, i.e., from input to output, then propagating errors backwards, and updating the weights according to the equation

$$\Delta_p W_{ij} = \epsilon \, \delta_{pj} O_{pi}$$

where p is an index identifying the member of the training set, $\Delta_p W_{ij}$ is the change in weight W_{ij} on training pattern p, ϵ is a constant known as the "learning rate," and δ_{pj} is given by

$$\delta_{pj} = - \, (\delta E_{pj}/dO_{pj}) \, TF'(A_{pj})$$

The error is E_{pj}, and $TF'(A_{pj})$ is the slope of the transfer function that relates the output, O_{pj}, of a neuron to its activation value, A_{pj}. The transfer function used in this application is known as a sigmoid function. It can be shown that

$$\delta_{pj} = TF'(A_{pj}) \, \Sigma_k \, \delta_{pk} \, W_{jk}$$

where jk refers to a weight between the hidden layer and the output layer. This then relates $\Delta_p W_{ij}$ to W_{jk} and effects the backward propagation. Training is stopped when the errors for all of the

7

output values are within specified bounds. This is normally taken to be within 10 % of their range. The range is scaled from the real world range to the range from 0 to 1.

For each training session, the network was started with completely random interconnections. The network was trained using data from cycle 7, which began in 1823, through cycle 21, which began in 1976. Data from cycles earlier than 7 were not used because of uncertainties in their accuracy. The triangles in Fig. 2 show the accuracy of the training achieved for the 15 cycles in the training set. If the neural network was perfectly trained, the points would fall on the straight line shown in the figure. On that line, the output of the neural network would equal the actual sunspot maximum observed.

The network operates in the range from 0 to 1 for all parameters. Real-world values must be scaled into this range. Sunspot numbers were scaled from the range 40 to 210 into the range 0 to 1, and the months were scaled from the range 30 to 80 into 0 to 1. In order to obtain convergence, the training criterion was set to 10% of the range, which corresponds to ±17 for the maximum sunspot number and ±5 months for the time to maximum. That means that the network was successfully trained only after it could output a sunspot maximum that was within ±17 of the actual sunspot maximum for each of the 15 cycles from cycle 7 through cycle 21.

The network was tested by removing one cycle at a time from the training set, retraining the network, and predicting the output parameters for the missing cycle. Thus 15 tests were conducted, one for each cycle from 7 through 21. The results of these tests are plotted as circles in Fig. 2. The standard deviation of the predictions of the sunspot maximum from the actual maximum for cycles 7 through 21 is 26.4. Generally the predictions fall outside of the values associated with the full training set, as expected. Note that the amplitude of cycle number 19, with the largest sunspot maximum, 201, is predicted no worse than the value associated with that cycle for the entire training set. The neural network is thus able to predict values that are larger than the values used in the training sets. However, it cannot predict values outside of its scaled range from 0 to 1.

Using all of the cycles from cycle 7 through cycle 21 to train the neural network and using the 3-month-smoothed data for the first 33 months of cycle 22 as input data, the neural network predicts the maximum sunspot number for cycle 22 to be 194 ±26 to occur 42 months (March 1990) after the minimum. The uncertainty in the prediction is taken to be the standard deviation of the difference between the predicted sunspot maximum and the observed sunspot maximum for the 15 test cases. This prediction is to be compared with the predictions for solar cycle 22 given in Table 2 of Withbroe [1989]. There the average value of the sunspot maximum
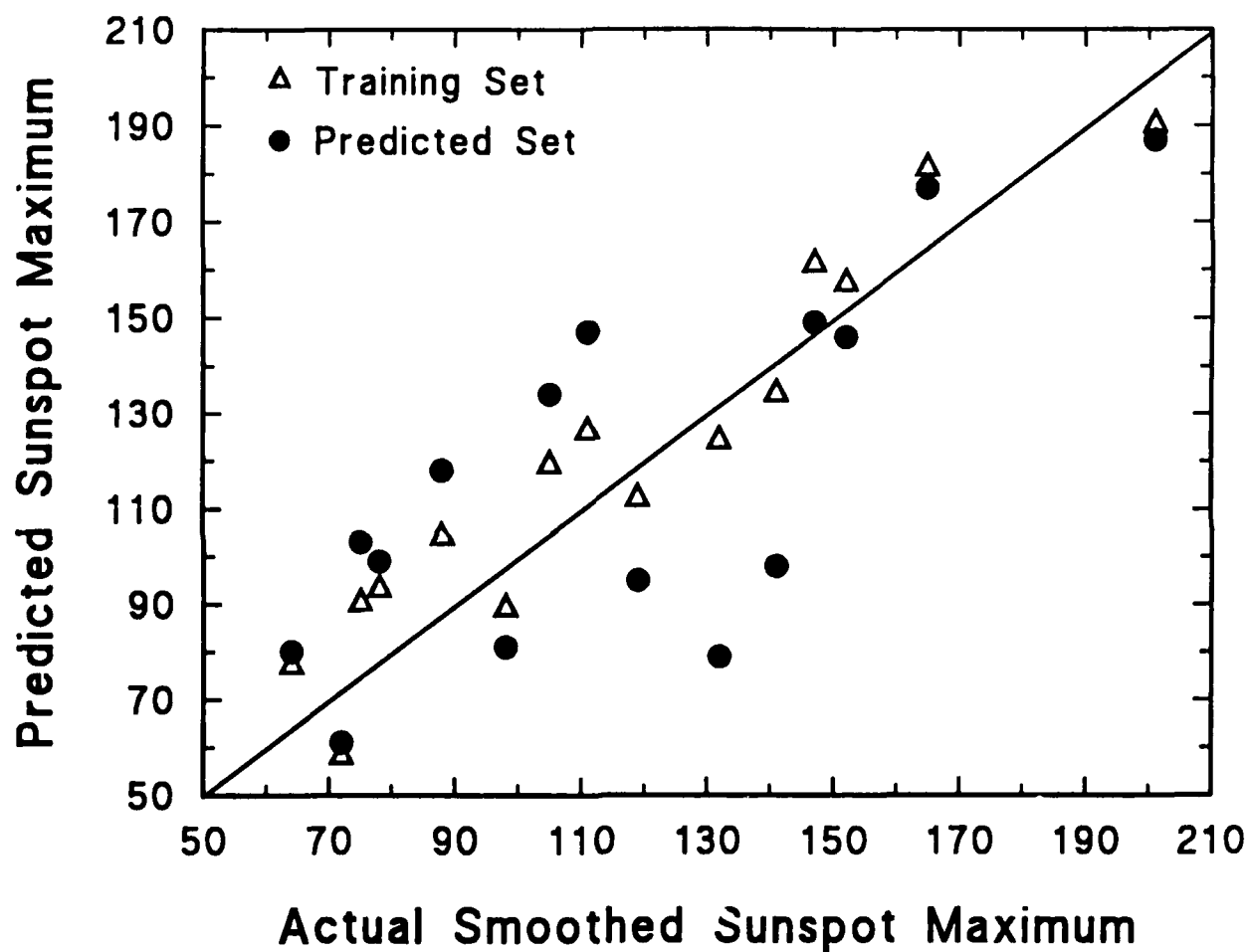
Fig. 2.   A Scatter Diagram Showing the Predicted Sunspot Maximum vs the Actual Sunspot
           Maximum for the Solar Cycles from 7 Through 21. The triangles include the entire training
           set used to predict the sunspot maximum for cycle 22. The circles show the prediction for a
           cycle when that cycle is removed from the training set.

for the statistical techniques is 94; for the precursor techniques, 1ɔ4; and for the McNish-Lincoln technique, 191.

The amplitude of cycle 22 was also predicted for each of the 15 test cases with one cycle removed. This should give an inferior answer. However the spread in the predictions should reflect the uncertainty in the predictions. The prediction using the full training set is centered at the cross in Fig. 3. The error bars shown are the standard deviation of the predictions from the actual values for the 15 test cases. The 15 predictions made with one cycle removed from the training set are plotted as triangles in Fig. 3. They range from 182.3 to 195.9 in amplitude with an average of 188.3 and from 37.6 to 48.3 months with an average of 41.0. In order to put the prediction into perspective with cycle 22, the actual values of the 13-month-smoothed sunspot numbers for cycle 22 are plotted as squares in Fig. 3. The solid squares show the data available at the time the neural network prediction was made. The open squares show the more recent data.
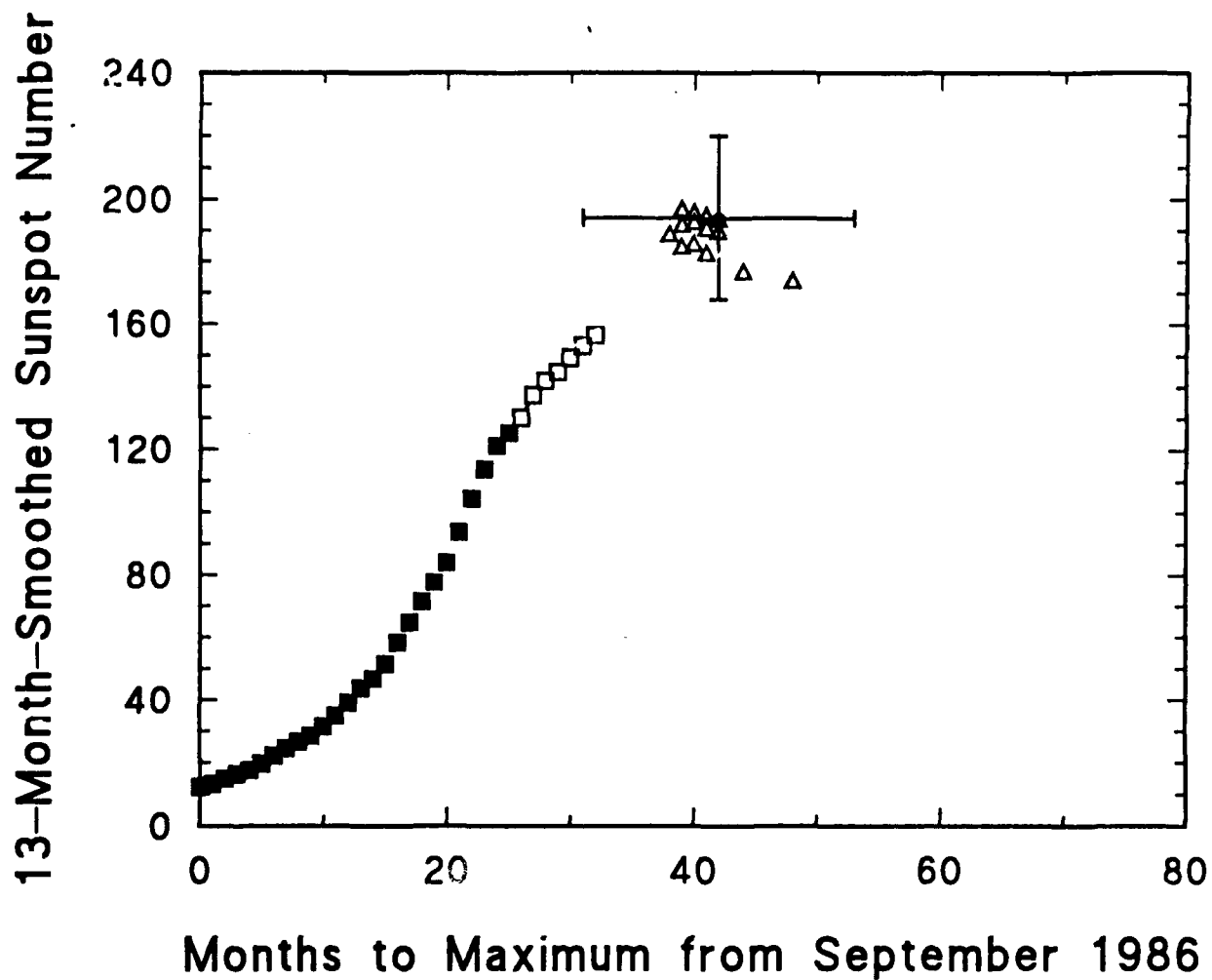
Fig. 3. The Prediction of the Maximum 13-Month-Smoothed Sunspot Number for Solar Cycle 22. The triangles show the predictions obtained as each cycle is individually removed from the training set. The squares show the actual values observed for cycle 22. The solid squares show the data available at the time the neural network prediction was made.

REFERENCES

McNish, A. G., and J. V. Lincoln, "Predictions of Sunspot Numbers," EOS. Trans. Am. Geophys. Union 30, 673 (1949).

Schatten, K. H., P. H. Scherrer, L. Svalgaard, and J. M. Wilcox, "Using Dynamo Theory to Predict the Sunspot Number During Solar Cycle 21," Geophys. Res. Lett. 5, 411 (1978).

Schatten, K. H., and S. Sofia, "Forecast of an Exceptionally Large Even-numbered Solar Cycle," Geophys. Res. Lett. 14, 632 (1987).

Withbroe, G. L., "Solar Activity Cycle: History and Predictions," J. Spacecraft and Rockets 26, 394 (1989).

LABORATORY OPERATIONS

The Aerospace Corporation functions as an "architect-engineer" for national security projects, specializing in advanced military space systems. Providing research support, the corporation's Laboratory Operations conducts experimental and theoretical investigations that focus on the application of scientific and technical advances to such systems. Vital to the success of these investigations is the technical staff's wide-ranging expertise and its ability to stay current with new developments. This expertise is enhanced by a research program aimed at dealing with the many problems associated with rapidly evolving space systems. Contributing their capabilities to the research effort are these individual laboratories:

Aerophysics Laboratory: Launch vehicle and reentry fluid mechanics, heat transfer and flight dynamics; chemical and electric propulsion, propellant chemistry, chemical dynamics, environmental chemistry, trace detection; spacecraft structural mechanics, contamination, thermal and structural control; high temperature thermomechanics, gas kinetics and radiation; cw and pulsed chemical and excimer laser development, including chemical kinetics, spectroscopy, optical resonators, beam control, atmospheric propagation, laser effects and countermeasures.

Chemistry and Physics Laboratory: Atmospheric chemical reactions, atmospheric optics, light scattering, state-specific chemical reactions and radiative signatures of missile plumes, sensor out-of-field-of-view rejection, applied laser spectroscopy, laser chemistry, laser optoelectronics, solar cell physics, battery electrochemistry, space vacuum and radiation effects on materials, lubrication and surface phenomena, thermionic emission, photosensitive materials and detectors, atomic frequency standards, and environmental chemistry.

Electronics Research Laboratory: *Microelectronics, solid-state device physics, compound semiconductors, radiation hardening; electro-optics, quantum electronics, solid-state lasers, optical propagation and communications; microwave semiconductor devices, microwave/millimeter wave measurements, diagnostics and radiometry, microwave/millimeter wave thermionic devices; atomic time and frequency standards; antennas, rf systems, electromagnetic propagation phenomena, space communication systems.*

Materials Sciences Laboratory: Development of new materials: metals, alloys, ceramics, polymers and their composites, and new forms of carbon; nondestructive evaluation, component failure analysis and reliability; fracture mechanics and stress corrosion; analysis and evaluation of materials at cryogenic and elevated temperatures as well as in space and enemy-induced environments.

Space Sciences Laboratory: Magnetospheric, auroral and cosmic ray physics, wave-particle interactions, magnetospheric plasma waves; atmospheric and ionospheric physics, density and composition of the upper atmosphere, remote sensing using atmospheric radiation; solar physics, infrared astronomy, infrared signature analysis; effects of solar activity, magnetic storms and nuclear explosions on the earth's atmosphere, ionosphere and magnetosphere; effects of electromagnetic and particulate radiations on space systems; space instrumentation.